

STOCHASTIC SIMULATION OF HIGH-FREQUENCY GROUND MOTIONS BASED ON SEISMOLOGICAL MODELS OF THE RADIATED SPECTRA

BY DAVID M. BOORE

ABSTRACT

Theoretical predictions of seismic motions as a function of source strength are often expressed as frequency-domain scaling models. The observations of interest to strong-motion seismology, however, are usually in the time domain (e.g., various peak motions, including magnitude). The method of simulation presented here makes use of both domains; its essence is to filter a suite of windowed, stochastic time series so that the amplitude spectra are equal, on the average, to the specified spectra. Because of its success in predicting peak and rms accelerations (Hanks and McGuire, 1981), an ω -squared spectrum with a high-frequency cutoff (f_m), in addition to the usual whole-path anelastic attenuation, and with a constant stress parameter ($\Delta\sigma$) has been used in the applications of the simulation method. With these assumptions, the model is particularly simple: the scaling with source size depends on only one parameter—seismic moment or, equivalently, moment magnitude. Besides peak acceleration, the model gives a good fit to a number of ground motion amplitude measures derived from previous analyses of hundreds of recordings from earthquakes in western North America, ranging from a moment magnitude of 5.0 to 7.7. These measures of ground motion include peak velocity, Wood-Anderson instrument response, and response spectra. The model also fits peak velocities and peak accelerations for South African earthquakes with moment magnitudes of 0.4 to 2.4 (with $f_m = 400$ Hz and $\Delta\sigma = 50$ bars, compared to $f_m = 15$ Hz and $\Delta\sigma = 100$ bars for the western North America data). Remarkably, the model seems to fit all essential aspects of high-frequency ground motions for earthquakes over a very large magnitude range.

Although the simulation method is useful for applications requiring one or more time series, a simpler, less costly method based on various formulas from random vibration theory will often suffice for applications requiring only peak motions. Hanks and McGuire (1981) used such an approach in their prediction of peak acceleration. This paper contains a generalization of their approach; the formulas used depend on the moments (in the statistical sense) of the squared amplitude spectra, and therefore can be applied to any time series having a stochastic character, including ground acceleration, velocity, and the oscillator outputs on which response spectra and magnitude are based.

INTRODUCTION

Recordings of high-frequency (greater than about 1 Hz) ground motions have two main uses: (1) they provide the seismologist with data basic for the understanding of source processes; and (2) they are used by engineers to derive the motions that structures must be designed to withstand. Of importance for either of these uses, even if not absolutely required, are methods for generating the ground motions for hypothetical earthquakes. While both engineers and seismologists recognize the stochastic nature of high-frequency ground motions, they estimate ground motions in fundamentally different ways (see Boore, 1983, for a collection of recent references). The engineer relies heavily on an empirical approach in which the motions are constructed so as to agree in essential ways (such as amplitude, frequency

content, and duration) with existing data (e.g., Iyengar and Iyengar, 1969; Nau *et al.*, 1982; the references therein). The actual methods for constructing the motions range from filtering and windowing Gaussian noise to adding together suitably scaled recorded accelerograms. These techniques might be called replicative or empirical models; they have a long history. Of more recent development are the predictive or physical models used by seismologists. These models usually involve either the prediction of the motions from a fault of specified dimension and orientation whose properties, such as slip or rupture velocity, vary randomly over the fault surface (e.g., Bouchon, 1978; Joyner and Boore, 1980), or the random superposition of the theoretical radiated fields from many circular patches, concentrated, in effect, at a point (e.g., Boatwright, 1982). The former is useful for site-specific simulations, whereas the latter captures the essence of the high-frequency motion at an average site from an average earthquake of specified size.

In this paper, I present a simple method that is a hybrid of the approaches taken by engineers and seismologists. The idea is to generate a time series of filtered and windowed Gaussian white noise whose amplitude spectrum approximates the acceleration spectrum given by physical considerations—in this case the Brune (1970) spectrum modified to remove frequencies above a certain cutoff frequency. A suite of accelerograms can be generated by varying the seed of a pseudo-random number generator, and various measures of the motion can be computed for comparison with data. With a prescribed stress parameter, the scaling with earthquake size at a given distance depends on only one parameter—seismic moment (or equivalently, moment magnitude). Surprisingly, this simple one-parameter scaling model provides a good fit to many measures of high-frequency strong ground motion, measures based on analysis of hundreds of strong-motion recordings.

This paper is not the first to use the Brune spectrum as the basis for explaining high-frequency motion; the idea was presented and elaborated on in a series of articles by Hanks and McGuire (Hanks, 1979a, 1979b; McGuire and Hanks, 1980; Hanks and McGuire, 1981). They were concerned with rms and peak accelerations. Using the simulation method presented here, I find that the same spectral model can also predict peak velocity, Wood-Anderson instrument response, and response spectra.

Hanks and McGuire used Parseval's theorem to predict the rms acceleration (a_{rms}) from the integral of the squared acceleration spectrum; they then used some results from random vibration theory to relate the a_{rms} to peak ground acceleration (a_{max}). This approach is much simpler and less costly (but potentially less exact) than simulating time series and measuring the peak motions. Using equations from Cartwright and Longuet-Higgins (1956), I have extended the random vibration predictions to peak velocity, Wood-Anderson response, and response spectra. The random vibration results are generally in excellent agreement with those from the simulated time series.

METHOD

The essence of the method is to generate a transient time series whose spectrum matches, at least as an ensemble average, a specified amplitude spectrum. This goal can be obtained in a number of ways. For example, first a window can be applied to a time sequence of random white noise with zero mean. Then the amplitude spectrum of this time series can be replaced by the desired spectrum, leaving the phase untouched. Transformation back to the time domain results in a transient time series whose amplitude spectrum exactly matches the specified spectrum.

Unfortunately, the forced shape of the amplitude spectrum can introduce narrow-band oscillations in the record. Another method starts with random phase and the given amplitude spectrum in the frequency domain. After transformation to the time domain, a suitably normalized window is applied to produce a transient signal. The window, however, distorts the spectrum; there is no assurance that the desired spectrum will be attained, even with an average over the ensemble of simulations. In a sense, these two approaches are end members of a range of methods trying to achieve two things: a time series of finite duration with a specified amplitude spectrum. The first method produces a time series that is only approximately of finite duration but does have the specified amplitude spectrum; the second method

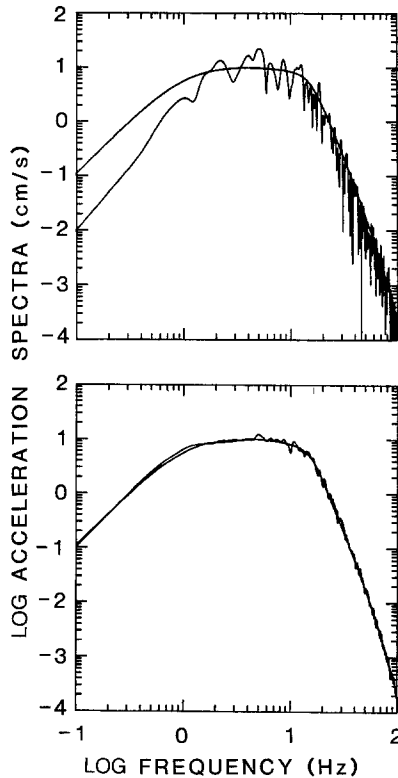


FIG. 1. Fourier amplitude spectrum of ground acceleration at 10 km from a magnitude 5 earthquake. (Top) Smooth curve: given spectra, jagged curve: spectra for one realization of the simulation process (Bottom) As above, but averaged over 20 simulations (the averaged spectrum is the square root of the arithmetic mean of the energy density spectrum).

achieves the converse. A third method, falling between the first two, does not suffer from the limitations of the first two methods; it is the basis for all the results in this paper. It starts with the windowing of a time sequence of band-limited random white Gaussian noise with zero expected mean and variance chosen to give unit spectral amplitude on the average (this criterion is met if the variance of the noise is equal to the total bandwidth, and if the window is normalized such that the integral of its square is unity). The spectrum of the windowed time series is multiplied by the specified spectrum, and transformation back to the time domain yields the final time series. An example of an individual, average, and desired spectrum for a particular earthquake is shown in Figure 1; time series will be shown later.

The application of this method requires the spectral shape as a function of earthquake size. Only the shear wave contribution to the strong motion is considered in this paper; in almost all cases it dominates the motion, particularly on the horizontal components of ground shaking. The form adopted here for the acceleration spectrum $A(\omega)$ of shear waves at a distance R from a fault with moment M_0 is

$$A(\omega) = C M_0 S(\omega, \omega_c) P(\omega, \omega_m) \frac{e^{-\omega R/2Q\beta}}{R} \quad (1)$$

where C is a constant given by

$$C = \frac{R_{\theta\phi} \cdot FS \cdot PRTITN}{4\pi\rho\beta^3}. \quad (2)$$

$R_{\theta\phi}$ is the radiation pattern, FS is the amplification due to the free surface, $PRTITN$ is the reduction factor that accounts for the partitioning of energy into two horizontal components (taken as $1/\sqrt{2}$ here), and ρ and β are the density and shear velocity. Following Aki (1967) and Brune (1970), the source spectrum S is given by

$$S(\omega, \omega_c) = \frac{\omega^2}{1 + (\omega/\omega_c)^2} \quad (3)$$

where ω_c is the corner frequency. The spectrum in equation (3) is that of the ω -squared model; some simulations were also made with an ω -cubed model in which the superscript 2 in the denominator was replaced by a 3. The $P(\omega, \omega_m)$ in equation (1) is a high-cut filter that accounts for the observation that acceleration spectra often show a sharp decrease with increasing frequency, above some cutoff frequency ω_m , that cannot be attributed to whole path attenuation [the whole path attenuation is accounted for by the exponential term in equation (1); frequency-dependent Q could be easily included if desired]. Papageorgiou and Aki (1983) have attributed ω_m to source processes and Hanks (1982) to attenuation near the recording site. The form for the high-cut filter P has arbitrarily been taken to be

$$P(\omega, \omega_m) = [1 + (\omega/\omega_m)^{2s}]^{-1/2} \quad (4)$$

where s controls the decay rate at high frequencies. Based on several observed spectra, s was assigned a value of 4.

Assuming that ω_m is not a function of earthquake size, the spectra for different earthquakes are controlled by two parameters: seismic moment (M_0) and corner frequency ($f_c = \omega_c/2\pi$). These two source parameters can be related through an equation involving another parameter with the dimensions of stress ($\Delta\sigma$)

$$f_c = 4.9 \times 10^6 \beta (\Delta\sigma/M_0)^{1/3} \quad (5)$$

where f_c is in Hertz, β is in kilometers/second, $\Delta\sigma$ is in bars, and M_0 is in dyne-cm (Brune 1970, 1971). Although originally derived from a relation between static stress drop, fault slip, and fault size, $\Delta\sigma$ is best thought of here as simply a parameter controlling the strength of the high-frequency radiation. It has been referred to in the literature by a variety of names, including effective stress, dynamic stress drop, and rms stress drop.

A transient accelerogram is obtained in the time domain by use of a shaping window whose length is controlled by the source duration (T_d). This simplistic procedure does not produce variations of the frequency content with time, but such variation is unimportant for the high-frequency ground motions of concern here. Following Hanks and McGuire (1981), T_d is related to the corner frequency by

$$T_d = f_c^{-1}. \quad (6)$$

Two windows have been used in this study, the simplest being a box of duration T_d . A more realistic accelerogram is obtained with the shaping window

$$w(t) = at^b e^{-ct} H(t) \quad (7)$$

where $H(t)$ is the unit-step function. Saragoni and Hart (1974) found that this window is a good representation of the averaged envelope of the squared acceleration time series. It is convenient to choose the shape parameters b , c such that: (1) the peak of the envelope occurs at some fraction ϵ of a specified duration T_w (not necessarily the end of the time series); and (2) the amplitude at time T_w is reduced to the fraction η of the maximum amplitude. These conditions yield

$$b = -\epsilon \ln \eta / [1 + \epsilon(\ln \epsilon - 1)] \quad (8)$$

and

$$c = b/\epsilon T_w. \quad (9)$$

The normalizing factor a can be chosen in several ways

$$a = (e/\epsilon T_w)^b \quad (10)$$

gives a maximum amplitude of unity, and

$$a = \left[\frac{(2c)^{2b+1}}{\Gamma(2b+1)} \right]^{1/2} \quad (11)$$

results in an envelope with unit squared area (Γ is the gamma function).

In all applications in this paper, η was chosen to be 0.05. With this choice, I found that $\epsilon = 0.2$ was consistent with values of a , b , and c obtained by Saragoni and Hart (1974) from fitting the envelope function to 22 strong-motion accelerograms. Setting $T_w = 2T_d$ gives a record whose duration of strong shaking (defined in the caption to Figure 2) is close to T_d , as was desired (Figure 2).

A flow chart outlining the method is given in Figure 3. As shown there, a suite of accelerograms can be generated by simply changing the seed of the pseudo-random number generator. Statistics of various measures of ground motion, such as peak acceleration, velocity, and Wood-Anderson instrument response, are collected for comparison with data.

MODEL VERIFICATION

Many methods have been proposed for simulating suites of accelerograms for use as input motions in assessments of site and structural response; the method proposed

here is unique in its combination of stochastic simulation and physically based spectral amplitudes and record duration. Although any spectral scaling law could be used, I have emphasized the scaling law obtained from the ω -squared model and Brune's relation between f_c , $\Delta\sigma$, and M_0 . This particular scaling law was chosen because of the success that Hanks and McGuire (1981) had with it in explaining observed peak and rms accelerations. A more thorough test of this scaling model is presented here by comparing simulated peak accelerations, peak velocities, response spectra, and Wood-Anderson instrument responses against values obtained from recent regression analyses of several hundred strong-motion recordings by Boore (1980) and Joyner and Boore (1981, 1982). The model is also tested against ground motions from aftershocks of the 1975 Oroville, California, earthquake and from small earthquakes recorded deep in a South African gold mine by McGarr *et al.* (1981).

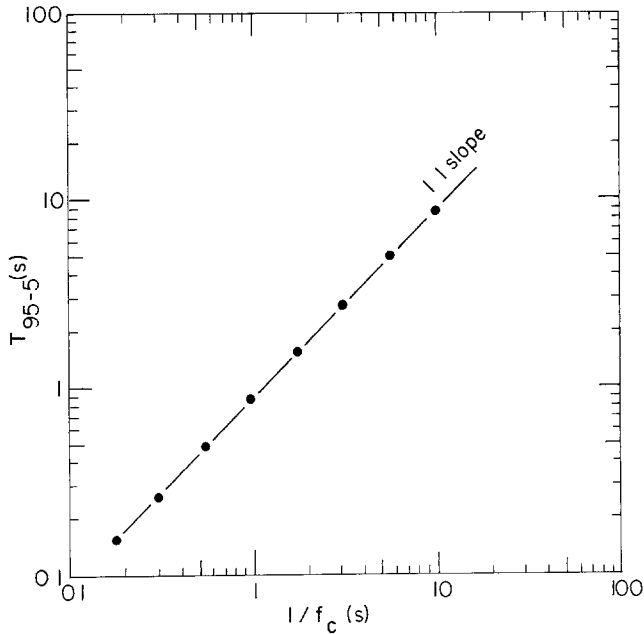


FIG. 2. Duration of simulations, defined as the time interval between the 95 and 5 per cent levels of the cumulative integral of acceleration squared, plotted as a function of inverse corner frequency.

Western North America ground motions. In the previous section, the spectral shape and amplitude were determined by a small number of parameters. If $f_m (= \omega_m/2\pi)$ is taken to be a path or site effect, the only source-dependent parameters are M_0 and $\Delta\sigma$ (or f_c). From an analysis of 16 California earthquakes, Hanks and McGuire (1981) found that $\Delta\sigma$ was about 100 bars (to within a factor of two) although the independently estimated static stress drops ranged from 6 bars to 140 bars. Because of this, I fixed $\Delta\sigma$ as 100 bars in the simulations, thus reducing the source dependence of the scaling law to only one parameter—seismic moment. The regression analyses against which the simulations will be compared used moment magnitude (M) rather than moment (M_0) as the measure of source size, and that has been done here as well. Moment magnitude is defined as

$$M \equiv 2/3 \log M_0 - 10.7 \quad (12)$$

(Hanks and Kanamori, 1979). All but one of the other parameters needed in the simulations were taken from Hanks and McGuire (1981): $\rho = 2.7 \text{ gm/cm}^3$; $\beta = 3.2 \text{ km/sec}$, $R_{\theta\phi} = 0.63$, $Q = 300$, $FS = 2$, and $PRTITN = 0.71$. The one exception was f_m : Hanks and McGuire related it to distance, Q , and instrument bandwidth (in the case of aftershocks of the 1975 Oroville, California, earthquake), but in a subsequent

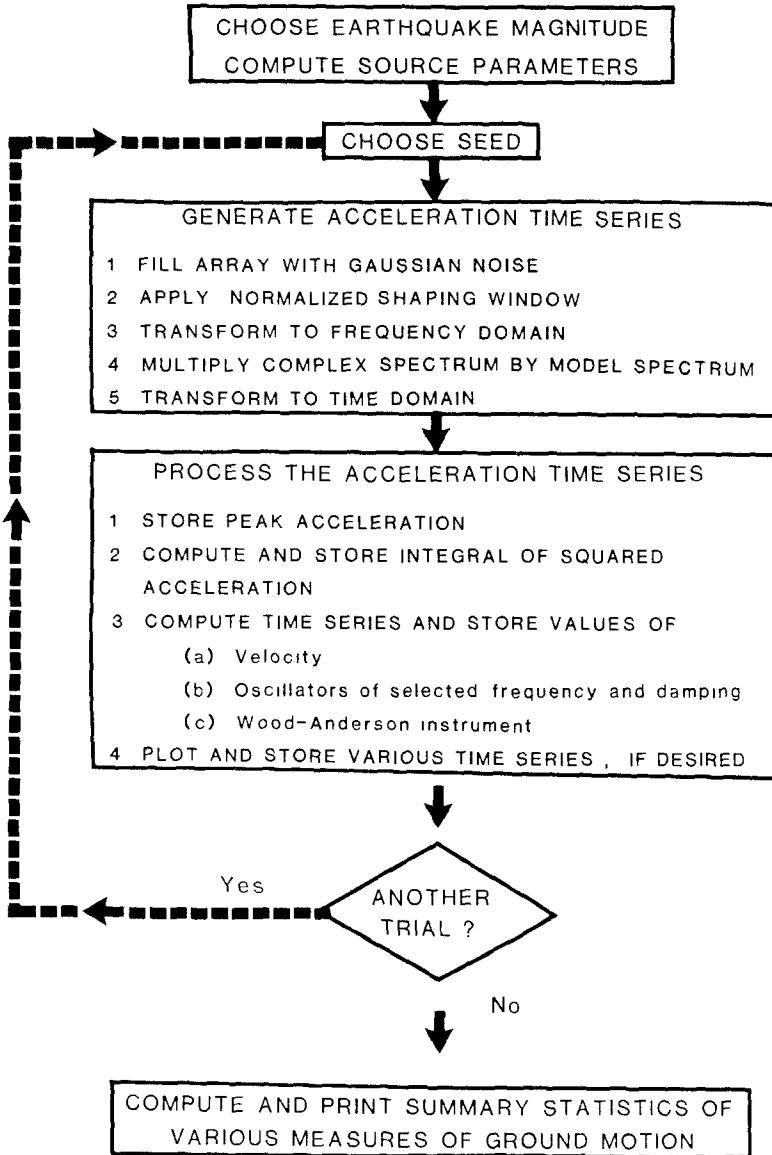


FIG. 3 Flow chart showing simulation technique used in this paper. Other techniques, briefly described in the text, lead to similar scaling of the various measures of ground motion.

paper Hanks (1982) noted that, at close distances, the spectra decayed much more rapidly with increasing frequency than predicted by the Q -term in equation (1). Based on conversations with T. Hanks, I have used $f_m = 15 \text{ Hz}$ (with some runs for $f_m = 7.5$ and 30 Hz).

It should be emphasized that the parameters in the simulations were not modified

to fit the data. On the other hand, 7 of the 16 earthquakes used by Hanks and McGuire (1981) also provided data in the regression studies of Joyner and Boore (1981, 1982) and therefore a certain degree of similarity might be expected between the simulations and the regression results. Joyner and Boore used data from up to 17 events, however, so the overlap between the studies is not great.

The majority of the comparisons between simulations and data will be made as a function of magnitude at a fixed distance of 10 km (in evaluating the equations of Joyner and Boore, r rather than d was set equal to 10 km). The empirically determined magnitude dependence comes from data that is mostly at distances beyond 10 km. The observed attenuation curves, derived within the context of a point source approximation such as used in the simulation model, was used to extrapolate the magnitude scaling to $r = 10$ km. As discussed by Joyner and Boore (1981, Appendix), the actual scaling close to large earthquakes would be somewhat different from that determined at distances of tens of kilometers. A distance of 10 km was chosen because I wished to emphasize the scaling with source strength. Comparisons at greater distances might be degraded by the inadequacy of the constant- Q model or the value adopted for Q .

Spectra of acceleration, velocity, and Wood-Anderson response are shown in Figure 4 for moment magnitudes from 4 to 7. These are the target spectra for the simulations. Examples of the acceleration, velocity, and Wood-Anderson time series are shown in Figure 5 for magnitudes of 4 and 7. The records have a reasonable appearance. Among other things, note the similarity between the velocity and Wood-Anderson traces, a similarity pointed out by Kanamori and Jennings (1978). The velocity spectra fall off less rapidly at high frequencies than do the Wood-Anderson spectra, thus explaining the enrichment of the former in high frequencies. Note also the simple character of the $M = 4$ Wood-Anderson record (and to a lesser extent the velocity record); even though the simulation method starts with a sequence of random numbers, the subsequent windowing and filtering can produce a nonrandom-appearing waveform.

These time series can be used in all manner of soil and structural response calculations (e.g., Boore and Joyner, 1983). The business of this section, however, is the comparison of various amplitude measures of the simulated ground motion with those obtained from analyses of data. The geometric means of the ground motion extrema were computed from 20 simulations at each magnitude. Two velocity traces were calculated for each magnitude: one by integration of the acceleration time series; the other by high-pass filtering of the first velocity trace. The filtering was intended to simulate the standard processing to which the strong-motion data are subjected. The difference in the velocity values is only important at magnitudes above about 7.0.

The peak accelerations and peak velocities from the simulations are shown in Figure 6, along with the regression curves of Joyner and Boore (1981, 1982). The regression curves are based on numerous strong-motion records from many earthquakes of magnitude 5 or greater located in western North America (the number of records used differs for the acceleration and velocity curves; furthermore, the 1982 study contains more velocity data, but fewer acceleration data, than the 1981 paper). For magnitudes above 5, the simulations define straight lines with slopes of 0.35 and 0.50 for acceleration and velocity; respectively. These lines are in reasonable agreement with the data, both in slope and in absolute level. Below magnitude 5, the simulations predict a steepening slope with decreasing magnitude. Unfortunately, the Joyner and Boore studies considered no earthquakes with magnitude

less than 5. Seekins and Hanks (1978), however, computed the average values of peak accelerations from aftershocks of the 1975 Oroville, California, earthquake, recorded at distances near 10 km. These average values, shown in Figure 6, are consistent with the simulation predictions. Later I will show that the simulation model gives a reasonable fit to peak velocities and accelerations from data recorded

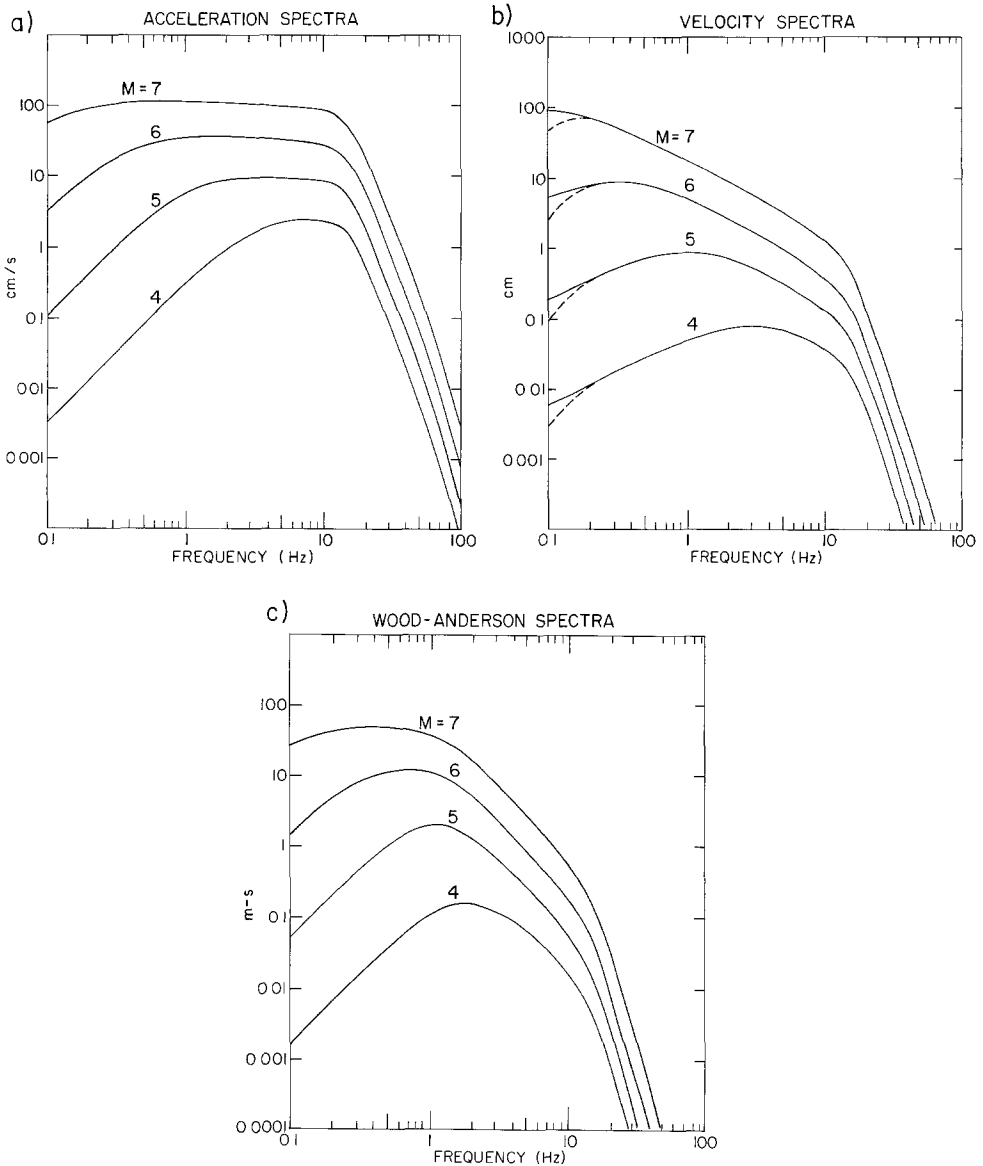


FIG. 4. Spectra of acceleration, velocity, and Wood-Anderson response at $R = 10$ km for the scaling model used in this paper ($\Delta\sigma = 100$ bars, $f_m = 15$ Hz). The dashed curves are the result of applying a two-stage Butterworth low-cut filter with a corner frequency of 0.10 Hz (see text).

in a South African gold mine by McGarr *et al.* (1981) for earthquakes with moment magnitudes from 0.4 to 2.4.

Pseudo-velocity response spectra (psrv) for 5 per cent damping at frequencies close to 0.5, 1, 3, and 8 Hz are shown in Figure 7. As with the peak acceleration and velocity, the simulations provide a fit to the data that is surprisingly good, consid-

ering the simplicity of the model. The discrepancy at the higher frequencies may be less significant than it appears. It is not increasing with frequency, and the curve based on data would be lowered in amplitude if raw, rather than smoothed regression coefficients had been used. It is interesting to note that both simulations and data show a nonlinear dependence on magnitude that decreases with increasing oscillator frequency (at least above a magnitude around 5). The primary reason for this is the interaction between the magnitude-dependent corner frequency and the fixed frequency band of the oscillator impulse-response. For example, the 1-Hz oscillator frequency—near the corner frequency for magnitude 5—is below f_c for smaller

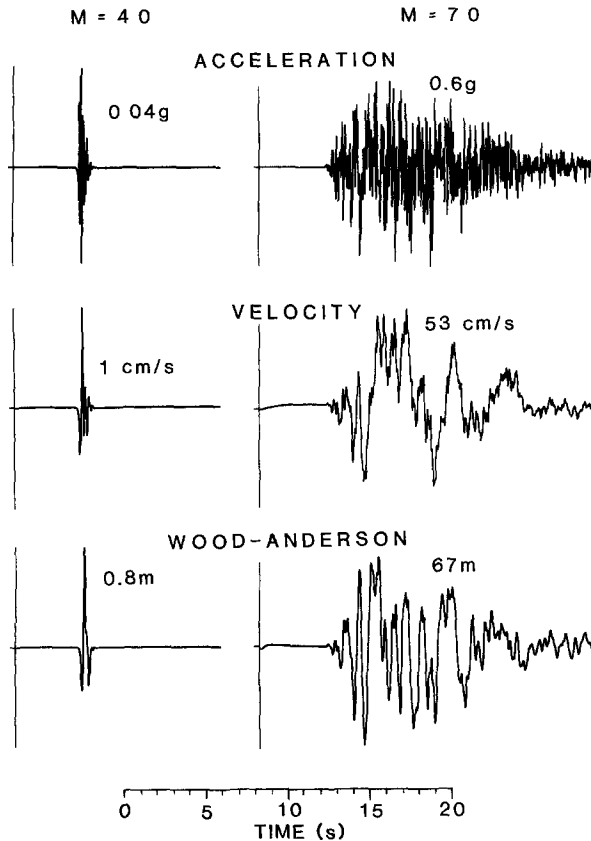


FIG. 5. Time series for magnitude 4 and 7 earthquakes. Peak motions are the average of peaks from 20 such time series. A low-cut filter with a cutoff frequency of 0.10 Hz has been applied to the velocity trace.

events and above it for larger ones. Because the acceleration spectrum at frequencies above f_c increases less rapidly with source size than at lower frequencies (Figure 4), the relation between the response spectrum and magnitude will have a steeper slope at small magnitudes than at larger magnitudes, thus leading to curvature in the scaling relation. The curvature in the dependence of peak acceleration and peak velocity on moment magnitude also depends on an interaction between characteristic frequencies in the model—in this case, the corner frequency f_c and the high-frequency cutoff f_m .

Although the peak acceleration, peak velocity, and response spectra data are all fit with a stress parameter equal to 100 bars, this must be taken in context with the

other parameters used in the simulations. For example, the average radiation pattern can vary by 10 to 20 per cent depending on whether equal weighting is used for the whole focal sphere and whether the rms or mean radiation pattern is computed. Furthermore, the simulations were compared with peak motions taken from the larger of the two horizontal components on each recording; the *PRTITN* factor of $1/\sqrt{2}$ used in the simulations is more appropriate for a peak motion chosen randomly

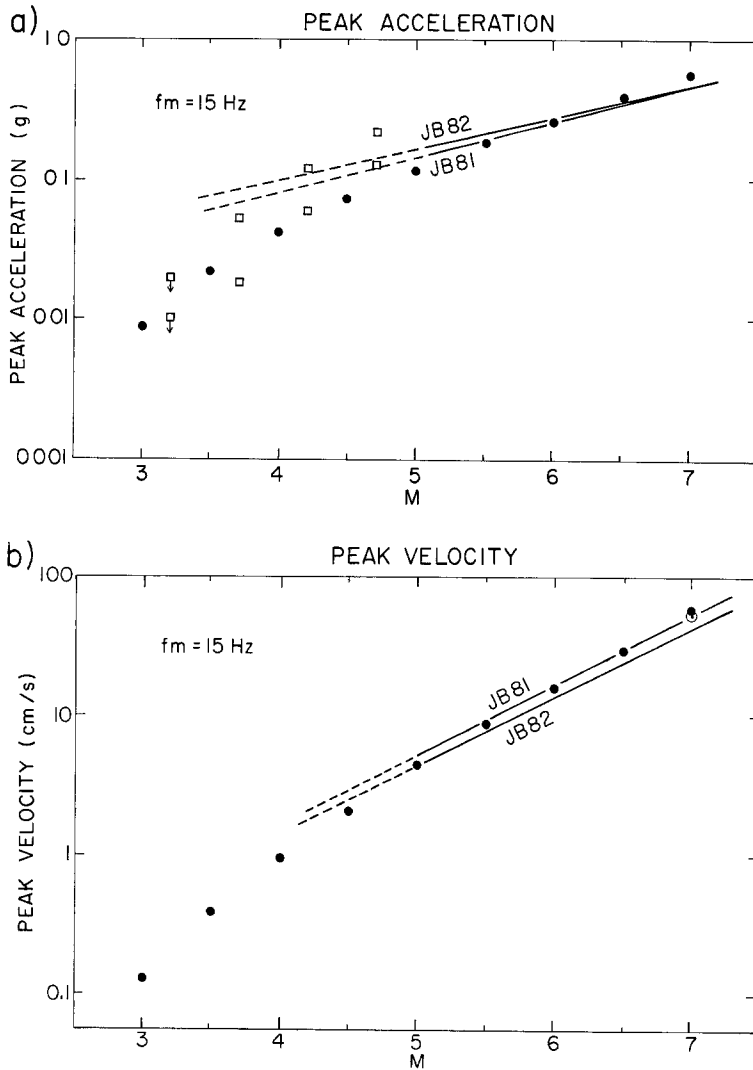


FIG. 6 Comparison of mean peak acceleration and peak velocity, derived from 20 simulations (circles), curves determined from regression studies of data (JB81: Joyner and Boore, 1981; JB82: Joyner and Boore, 1982), and peak accelerations from aftershocks of the 1975 Oroville, California, earthquake (open symbols, from Seekins and Hanks, 1978). No data from earthquakes less than magnitude 5 were used in the regression analyses, and therefore the curves have been dashed for $M < 5$. The upper points from the Oroville aftershocks correspond to rock sites, the lower to soil sites. As indicated by the arrows, the aftershock data for $M = 3.2$ are upper bounds because many events did not trigger the accelerographs. Seekins and Hanks (1978) assigned peak accelerations of $0.005 g$ to these events when computing the averages shown. The uncertainty in the estimates of peaks from simulations ranges from about 0.05 log units at small magnitudes to about 0.02 log units at large magnitudes. Open circles come from the series filtered to remove frequencies less than about 0.10 Hz; solid circles come from the unfiltered records. Only for peak velocity from a $M = 7$ event does the peak motion from the filtered and unfiltered records differ enough to show up separately on the figure.

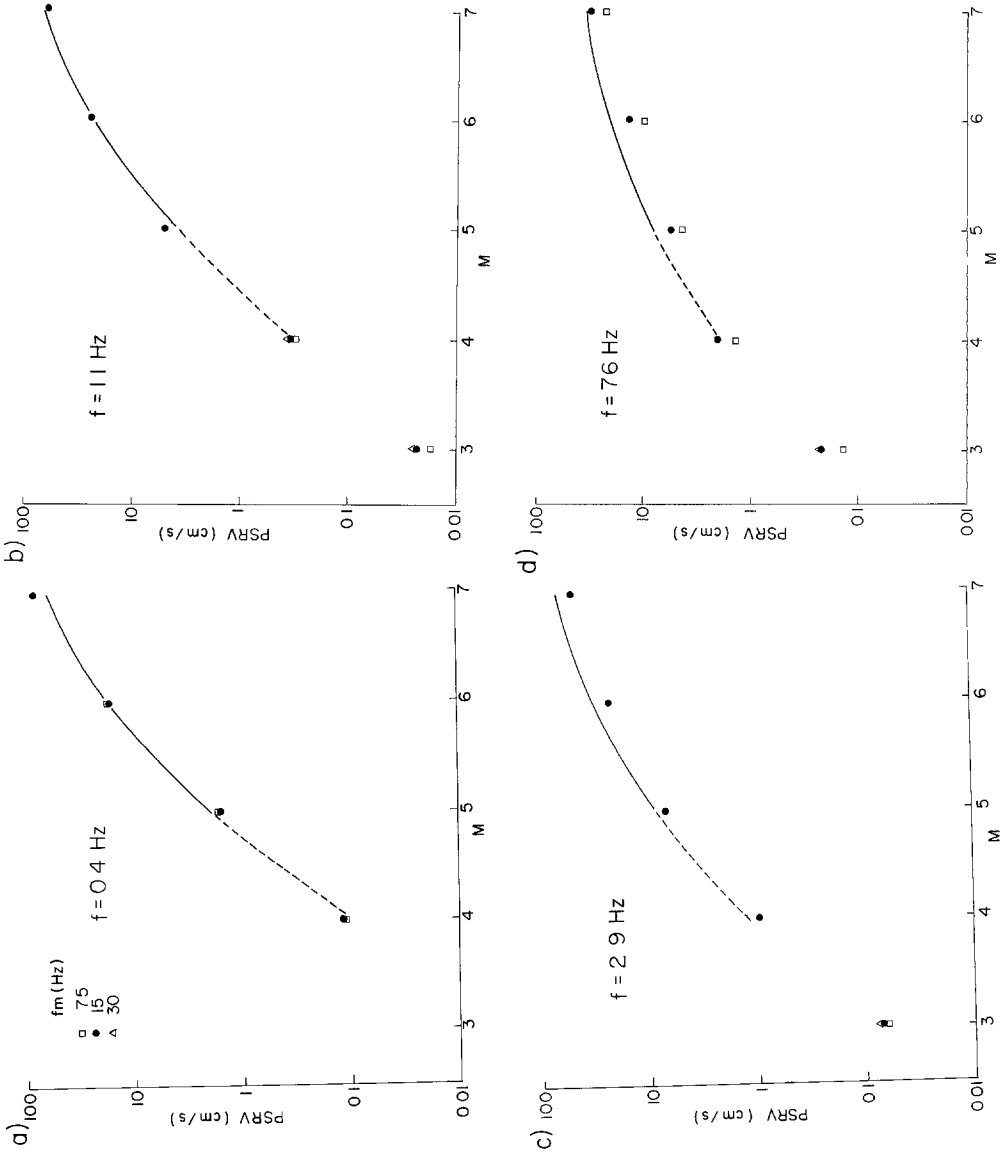


FIG. 7 Five per cent damped pseudo-relative velocity response spectra as a function of magnitude for frequencies of 0.4, 1.1, 2.9, and 7.6 Hz. Curves from regression equations in Joyner and Boore (1982), dashed for magnitudes not included in their data set. Symbols are from simulations with three values of the high-frequency cutoff f_m . When missing from plot, open symbols are indistinguishable from solid circles.

from the two horizontal components. The difference in the regression curves based on the two definitions of peak motion can be over 10 per cent (Campbell, 1981). Because of these factors, all that can be said about the stress parameter is that a value of 100 bars is consistent with the data when the other parameters are as given below equation (12).

The final strong-motion parameter to be checked for the western North America data is the Wood-Anderson instrument response. There are several ways of checking the simulated response of a Wood-Anderson instrument with the data. Because the distance attenuation aspects of the model have been deemphasized in this paper, and because the attenuation curve used in calculating local magnitudes may not be correct within a few tens of kilometers of the fault (Luco, 1982; Jennings and Kanamori, 1983). I have chosen to study the relation between peak velocity and Wood-Anderson response determined from the same accelerogram. In an earlier paper (Boore, 1980), I found that the peak velocity (v_{\max}) and one-half the maximum peak-to-peak amplitude from a Wood-Anderson instrument (A_{wa}) subjected to the same ground motion were related by the equation

$$v_{\max} = 0.77A_{wa} \quad (13)$$

where v_{\max} is in centimeters/second, and A_{wa} is in meters. The data leading to this correlation are shown in Figure 8. Most of the data are from events with magnitudes between 5 and 7. A similar one-to-one correlation between v_{\max} and A_{wa} has been found by Mahdyian and Singh (written communication, 1983) for smaller earthquakes—aftershocks of the 14 March 1979, Petatlan earthquake in Mexico having local magnitudes between 1.0 and 4.0. The coefficient in their correlation, however, is 1.58 rather than 0.77. There is no inconsistency in this result, for the simulations are in excellent agreement with both observed correlations (Figure 9), indicating that a difference in coefficients is expected. The change from one correlation to the other occurs for earthquakes whose corner frequencies are near the Wood-Anderson instrument corner frequency. In judging the results in Figure 9 a caveat is in order, however: the simulations are for a suite of earthquakes at one distance, but the data are from earthquakes of various sizes recorded over a wide range of distances. Thus, some of the small motions in Figure 8 are from large earthquakes at great distances, rather than small earthquakes at close distances. Therefore, the spectral shapes and dominant frequencies of the data and simulations contributing to the same range of ground motions in Figures 8 and 9 may differ significantly. Analysis of more data close to large earthquakes will show whether this is an important effect or not.

Because the Wood-Anderson response is obtained by multiplying the ground motion spectrum by the appropriate instrument response, and because the velocity and Wood-Anderson spectra have somewhat similar shapes for larger magnitude earthquakes (at least relative to acceleration and displacement spectra), it is natural to suppose that the relation $v_{\max} = 0.77 A_{wa}$ may depend almost entirely on the instrument response and therefore have little value in discriminating among various source models. This supposition can be ruled out for several reasons. First, simply evaluating the ratio of the velocity and Wood-Anderson spectra at the instrument corner frequency yields $v_{\max} = 0.45 A_{wa}$. Second, and more importantly, the simulations from neither a coherent source model nor a stochastic ω -cubed model (both described more fully later in the paper) lie on the $v_{\max} = 0.77 A_{wa}$ line (Figure 9). It is interesting to note, however, that all the models agree with one another at small

amplitudes, corresponding to small earthquakes. As shown in Figure 5, for these earthquakes the velocity and, in particular, the Wood-Anderson response has a simple pulse-like character. Therefore, the stochastic model should be expected to be similar to the coherent model for small earthquakes.

South Africa data. The most important test of the simulation model is the demonstration that it predicts ground motions in agreement with data from potentially damaging earthquakes (generally, those with moment magnitudes larger than

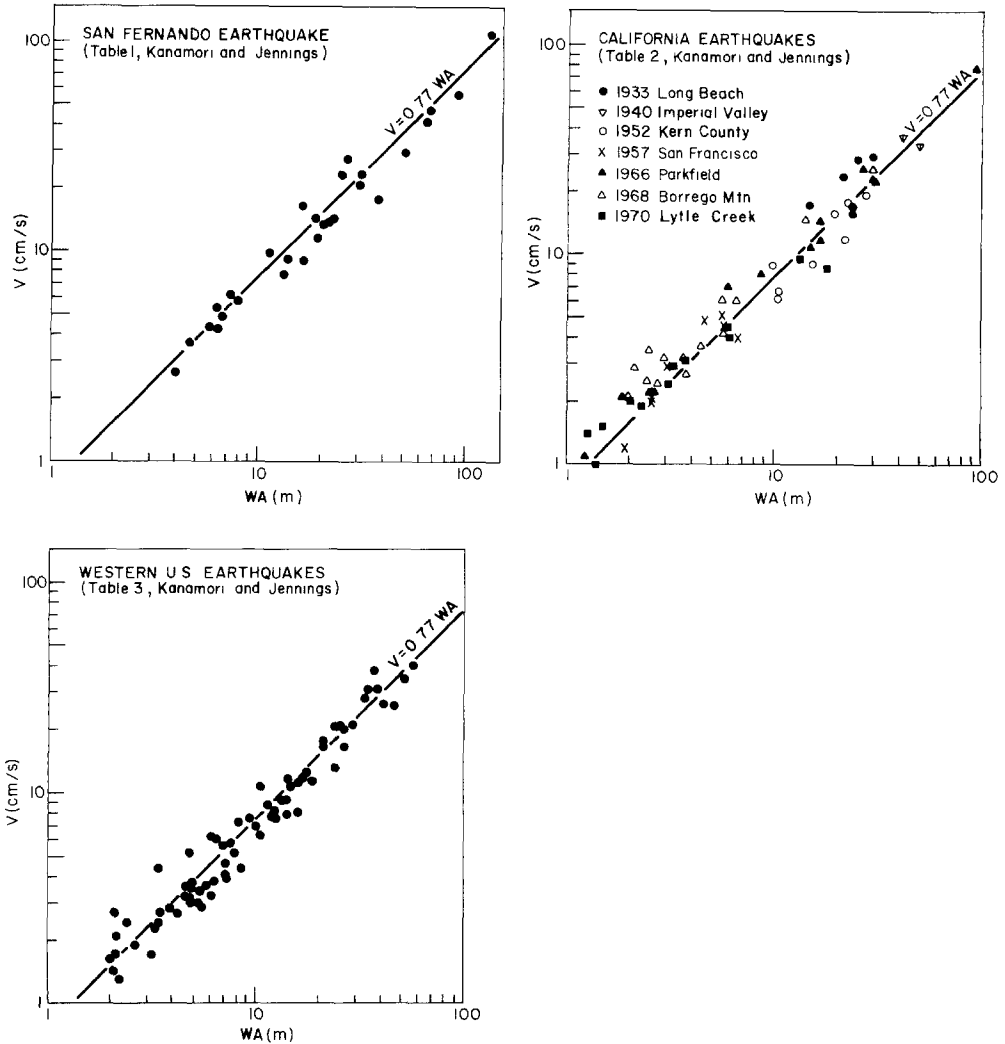


FIG. 8 The correlation between peak velocity and one-half of full range excursion of Wood-Anderson instrument response (from Boore, 1980, who used Wood-Anderson amplitudes computed by Kanamori and Jennings, 1978).

5.0). Most of the data used in the model verification came from earthquakes in California. Checking the model against data from smaller earthquakes is of seismological interest, however. The South African data tabulated by McGarr *et al.* (1981) provides an interesting test of the model, for the data were from small earthquakes recorded in a mine within competent rock ($\beta = 3.8$ km/sec) in a different tectonic environment than California. McGarr *et al.* (1981) computed the peak accelerations and velocities of the vector motions from accelerograms high-

cut filtered at 400 Hz. For consistency with the data processing, the free surface (*FS*) and energy partition (*PRTITN*) factors were taken as unity and the high-frequency cutoff (f_m) was 400 Hz in the simulations. From McGarr *et al.* (1981) and McGarr (oral communication, 1983), $\beta = 3.8$ km/sec and $Q = 600$. The simulations were made at a distance of 200 m, approximately the median distance for the data, and the data were normalized to that distance by assuming R^{-1} geometrical spreading. The comparison of the model predictions with the data are shown in Figure 10. A stress parameter of 50 bars was used, and no attempt was made to fine tune this parameter. This value of stress is in the middle of the range of stress drops determined for the events. In view of the scatter in the data and the simplicity of the model, the fit is very good. McGarr *et al.* (1981) also showed that the data could be fit by a simple source model—in their case by a coherent source model similar

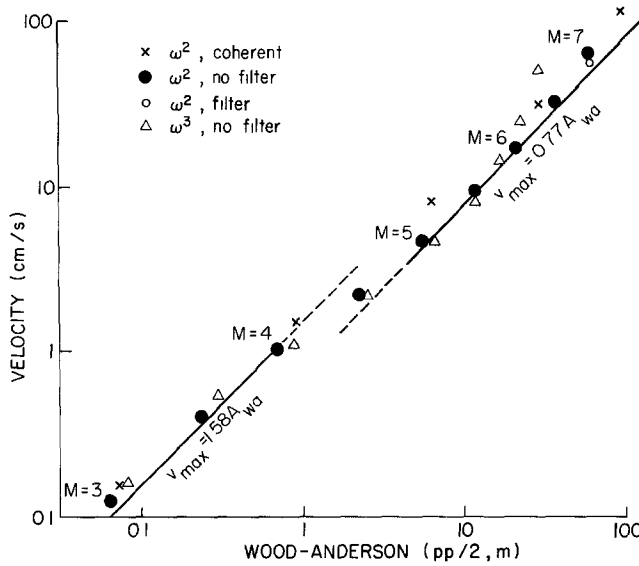


FIG 9 Observed (lines) and simulated (symbols) correlation between peak velocity and Wood-Anderson instrument response. Simulations were made at 10 km for M ranging from 3 to 7 in steps of 0.5 units (except for crosses, evaluated at whole steps) Magnitudes shown correspond to stochastic ω^2 model. Lines are solid in magnitude range used in their deviation; dashed extrapolations shown to emphasize offset. Peak values from low-cut filtered and unfiltered motions are generally indistinguishable. Wood-Anderson amplitudes are one-half the maximum range of motion ($pp/2$).

to one to be discussed shortly. The stochastic model, however, gives a better simultaneous fit to both the peak accelerations and peak velocities, and predicts a stronger dependence of the peak velocity on moment magnitude, in agreement with the data.

CONSTRAINTS ON f_m AND THE ω -SQUARED MODEL

The bandwidth of the acceleration spectrum is controlled by the corner frequency, f_c , and, at least at close distances, by f_m . The simulations have assumed that f_m is fixed, while f_c varies according to equation (5). To illustrate the effect of f_m , simulations were made for $f_m = 7.5, 15,$ and 30 Hz (Figures 7 and 11). As expected, measures of ground motion dominated by frequencies significantly less than f_m are not sensitive to f_m (e.g., v_{max} in Figure 11 and the first three psrv curves in Figure 7). The simultaneous fit of the model to both peak velocity and peak acceleration seems to exclude f_m as low as 7.5 Hz as an average value for the western North American data; the best fit is achieved with f_m near 15 Hz (Figure 11). At greater distances, the Q -attenuation may produce an effective f_m less than this.

The effect of f_m on peak acceleration is to produce an increasing difference in peak accelerations with decreasing magnitude for sites having different f_m (Figure 11). As pointed out to me by Hanks (oral communication, 1983), the aftershock data of the 1975 Oroville earthquake shown in Figure 6 show a similar divergence (excluding the biased values for $M = 3.2$), with the rock sites showing less magnitude dependence than the soil sites. Because the rock sites have a higher f_m than the soil sites (Hanks, 1982), the data are in qualitative accord with the simulations.

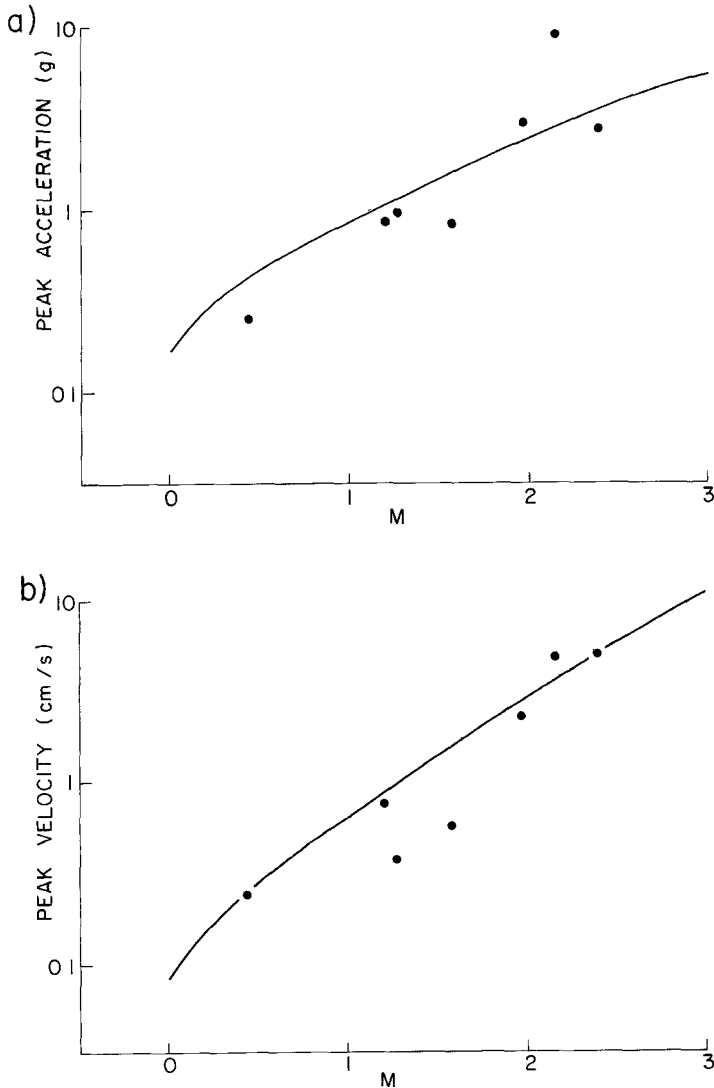


FIG. 10. Comparison of peak accelerations and velocities from South African accelerograms, from McGarr *et al* (1981), and simulations (using $f_m = 400$ Hz and $\Delta\sigma = 50$ bars). The simulations are represented by the smooth curves, the data by dots.

The comparison between simulations and data indicates that many amplitude measures of strong ground motion are consistent with an ω -squared model with constant stress parameter. Would another model do as well? The simulation method is not dependent on the specific model and therefore can be used to check any proposed model. No attempt has been made to do an extensive search of model

space, but for illustration I have considered the ω -cubed model obtained by replacing $(\omega/\omega_c)^2$ with $(\omega/\omega_c)^3$ in equation (3). As expected, it is not possible to match both the acceleration and velocity data with this model; if the stress parameter is adjusted to produce a fit to the velocity, the extra factor of ω/ω_c in the denominator of the ω -cubed model leads to an underestimation of the peak acceleration (Figure 12).

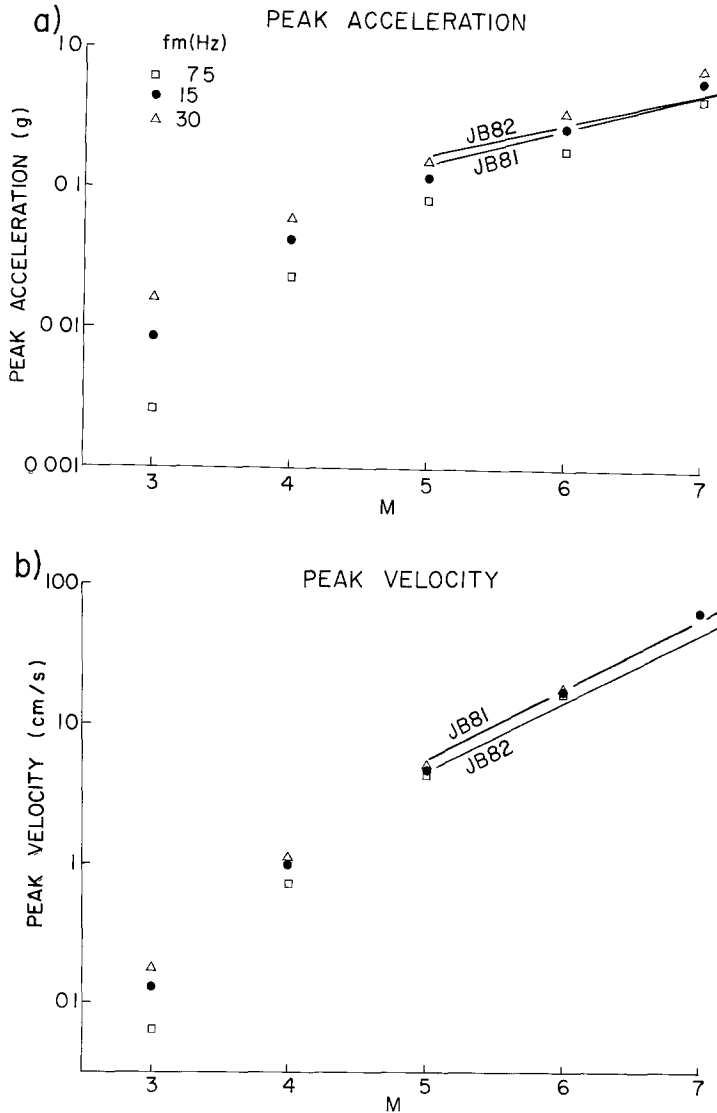


FIG. 11. Magnitude scaling of simulated peak ground accelerations and velocities for three values of f_m . The regression curves of Joyner and Boore (1981, 1982) are shown for reference.

COHERENT VERSUS STOCHASTIC MODELS

Although simple visual inspection of strong-motion records demands a stochastic source model (where I am lumping together source effects and any complexities introduced by the propagation path), the simulations were repeated with a coherent pulse based on the Brune (1970) far-field model. This comparison emphasizes the scaling of the peak motions with magnitude. The acceleration time series in the

“coherent model” (as defined here) corresponds to a doubly differentiated, filtered version of the far-field displacement pulse of Brune [1970, equation (37) with stress drop and source dimension variables replaced by seismic moment and corner frequency]. The displacement pulse is given by

$$u(t) \sim M_0 f_c^2 t e^{-2\pi f_c t} H(t) \tag{14}$$

where $H(t)$ is the unit-step function. The pulse is high-cut filtered according to

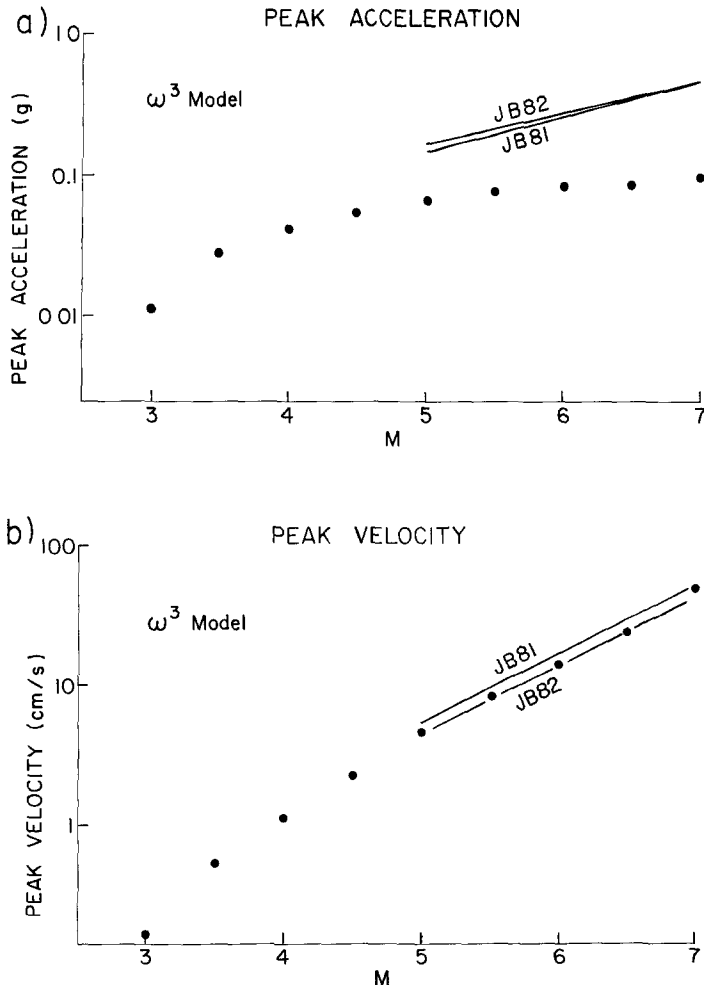


FIG. 12. Magnitude scaling of peak acceleration and velocity for simulations using an ω -cubed model. A scaling factor was used that brought the simulated peak velocities into approximate agreement with those from the data. Clearly, the ω -cubed model cannot fit the peak acceleration and peak velocity data simultaneously.

equation (4). For any magnitude, the amplitude spectrum of the coherent pulse and the ensemble average of the stochastic simulations are the same [given by equation (1)]; the difference lies in the phase spectrum. The scaling of peak acceleration and velocity with moment magnitude, based on the time-domain simulations, is shown in Figure 13.

The scaling factor $M_0 f_c^2$ in equation (14) controls the peak amplitudes of both

the velocity and acceleration traces for the coherent model. This means that for a fixed f_m both v_{max} and a_{max} scale the same way with magnitude (this was also predicted for the Brune model by McGarr *et al.*, 1981). Furthermore, if the stress

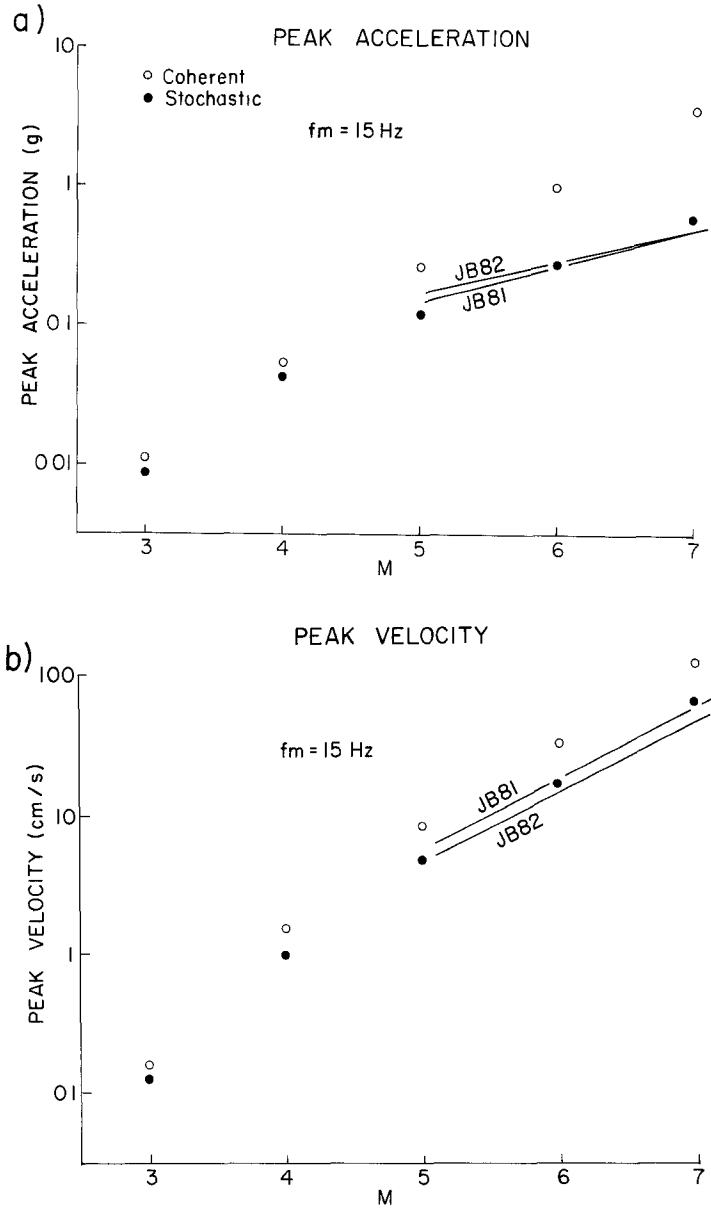


FIG. 13 Comparison of magnitude scaling for the coherent and stochastic source models, with $f_m = 15$ Hz. The regression curves of Joyner and Boore (1981, 1982) are shown for reference.

drop is constant, equations (5) and (14) can be combined to predict the scaling

$$\log\left(\frac{a_{max}}{v_{max}}\right) \sim \frac{1}{3} \log M_0 \tag{15}$$

and, using the definition of moment magnitude, the scaling for the coherent model

becomes

$$\log\left(\frac{a_{\max}}{v_{\max}}\right) \sim 0.5M \quad (16)$$

[Herrmann and Goertz, 1981; however, predict $\log(a_{\max}) \sim 0.0M$ rather than $\log(a_{\max}) \sim 0.5M$ for an ω -squared, constant stress drop, coherent model. This apparent inconsistency is explained by the high-cut filter they employed; the f_m in their model is not fixed, but decreases with increasing magnitude.]

A good approximation to the scaling of peak motions can be derived analytically for the stochastic model. When f_m/f_c is large (a good assumption for the larger earthquakes), the results are

$$\log(a_{\max}) \sim 0.3M \quad (17a)$$

and

$$\log(v_{\max}) \sim 0.5M \quad (17b)$$

(Hanks and McGuire, 1981, and Appendix A).

The simulation results are generally in good agreement with the analytical formulas for both the stochastic and coherent models (Figure 13). Furthermore, the scaling of peak velocity is similar for both the coherent and stochastic models. In contrast to the coherent model, however, the stochastic model predicts that peak acceleration has a weaker dependence on magnitude than does peak velocity. This agrees with observational results, and corroborates the expectation that a stochastic source model is needed to explain high-frequency ground motions.

The different magnitude scaling of the coherent and stochastic models is most likely due to the character of the waveforms. In the coherent model, the peak acceleration comes from a single sharp spike whose width is independent of magnitude. In contrast, the peak in the stochastic model can occur throughout a source duration T_d that increases with magnitude. The constraint that the spectra for both models be the same then requires that the peak accelerations of the stochastic model increase less rapidly with magnitude than in the coherent model. In essence, the number of peaks contributing to the spectrum is fixed in the coherent model but increases with magnitude in the stochastic model. At first glance it seems that this would also be the case for the peak velocity. While this is true to some extent, the peak velocity of the coherent model is carried by a pulse whose width increases with magnitude. The same considerations also explain why the peak motions from the coherent model are larger than those from the stochastic model—that are fewer peaks contributing to the spectrum in the coherent model.

RANDOM VIBRATION THEORY

Hanks and McGuire (1981) did not generate time series corresponding to a given amplitude spectra, as I have done. Instead, they used the following equation based on random vibration theory (Vanmarcke and Lai, 1980) to predict the peak acceleration from the rms acceleration

$$\frac{a_{\max}}{a_{rms}} = [2 \ln(N)]^{1/2} \quad (18)$$

where N is the number of extrema in a time interval T . Equation (18) is based on the assumption of a stationary time series with uncorrelated peaks, an assumption that is not strictly true in accelerograms. In general,

$$N = 2\tilde{f}T \tag{19}$$

where \tilde{f} is the predominant frequency of the motion (the constant “2” appears because two extrema are present in each cycle of motion, a factor sometimes overlooked—e.g., Udwadia and Trifunac, 1974, p. 213). Hanks and McGuire (1981) take

$$\tilde{f} = f_m. \tag{20}$$

Clearly, if equation (18)—or something similar—were adequate for the earthquake magnitudes of interest, its use would be preferable to the simulation method proposed here, at least for those applications not needing a time series. In this section, I compare the predictions from random vibration theory with the simulations. Several equations similar to equation (18) have been tested. Cartwright and Longuet-Higgins (1956) showed that equation (18) is an approximation valid for large N . For smaller N they gave an integral expression for the ratio of peak to rms [their equation (6.8)]. The integrand of their integral can be expanded by the binomial series and integrated term by term, yielding

$$\frac{E(a_{\max})}{a_{rms}} = \sqrt{\frac{\pi}{2}} \sum_{l=1}^N (-1)^{l+1} \frac{C_l^N}{\sqrt{l}} \xi^l \tag{21}$$

where $E(a_{\max})$ is the expected value of the largest of N acceleration extrema and C_l^N are binomial coefficients ($= N!/l!(N - l)!$). ξ is a measure of the bandwidth of the spectrum, given by

$$\xi = m_2/(m_0 m_4)^{1/2} \tag{22}$$

where m_0 , m_2 , and m_4 are the zeroth, second, and fourth moments of the energy density spectrum, respectively; ξ approaches unity with decreasing bandwidth. The k th moment is defined as

$$m_k = \frac{1}{\pi} \int_0^\infty \omega^k |A(\omega)|^2 d\omega. \tag{23}$$

For large values of N , Cartwright and Longuet-Higgins (1956; see also Davenport, 1964; Clough and Penzien, 1975) derive the following asymptotic expression

$$\frac{E(a_{\max})}{a_{rms}} = [2 \ln(N)]^{1/2} + \gamma/[2 \ln(N)]^{1/2} \tag{24}$$

where $\gamma = 0.5772 \dots$ (Euler’s constant). This equation is a good approximation to equation (21), even for small values of N . Note that equation (18), used by Hanks and McGuire, is the first term of the asymptotic expansion; the error in ignoring

the second term is about 10 per cent for $N = 20$. Other equations relating rms and peak acceleration have been derived by Vanmarcke (1976) and Udawadia and Trifunac (1974); listed in Appendix B, they differ from the equations above by including a probability parameter so that confidence limits can be derived. Regardless of the equation used, a_{rms} , N , and T must be estimated. For T , I use the earlier equation (6) equating T to the inverse of the source corner frequency. From Parseval's theorem, a_{rms} is given by

$$a_{rms} = (m_0/T)^{1/2}. \quad (25)$$

Finally, equation (19) is used to estimate N . This in turn requires the predominant frequency \tilde{f} . In equation (21), N is the number of extrema, and the appropriate frequency is

$$\tilde{f} = \frac{1}{2\pi} (m_4/m_2)^{1/2}. \quad (26)$$

For the asymptotic form [equation (24)], N is the number of zero crossings, given by equation (19) with

$$\tilde{f} = \frac{1}{2\pi} (m_2/m_0)^{1/2}. \quad (27)$$

The equations above show that after choosing the duration T , the relation between maximum amplitudes and rms amplitudes depends only on moments of the ground motion spectrum. There is nothing restricting their use to ground acceleration; in particular they can be applied to the ground velocity and response spectra as long as the basic assumptions of stationarity and uncorrelated peaks are not strongly violated.

Although working in terms of the integral measures m_k allows for generality in the random vibration predictions, analytical approximations can sometimes be made that are useful in predicting explicitly the dependence of the peak motions on the source parameters (as, e.g., Hanks and McGuire, 1981, have done for peak acceleration). This has been done in Appendix A for peak acceleration and peak velocity.

Various measures of ground motion as predicted by the time series simulations and by the random vibration theory are compared in Figures 14 and 15. In general, the random vibration theory is adequate for predicting the ground motion. The divergences from the simulations occur when N is small (I have constrained it to be 2 or greater). The theory also begins to break down when the successive peaks are strongly correlated, in violation of an assumption made in the theory. These failures are of little consequence in most cases, however, and modifications to the theory that account for the specific shape of the window function could probably be made. The extensions of the theory to response spectra could also remove the uncertainty in specifying the duration of the oscillator response. Although for the computations shown in Figure 15 I have assumed it to be equal to the duration of the ground motion, the oscillator duration will be longer than that. The effect on predicted ground motion values of underestimating the response duration will be

most conspicuous when the oscillator periods are longer than the source duration (see note 1 added in proof).

The conclusion from all of this is that in most cases, the asymptotic formula [equation (24)] does an excellent job of predicting peak motions. It is convenient to

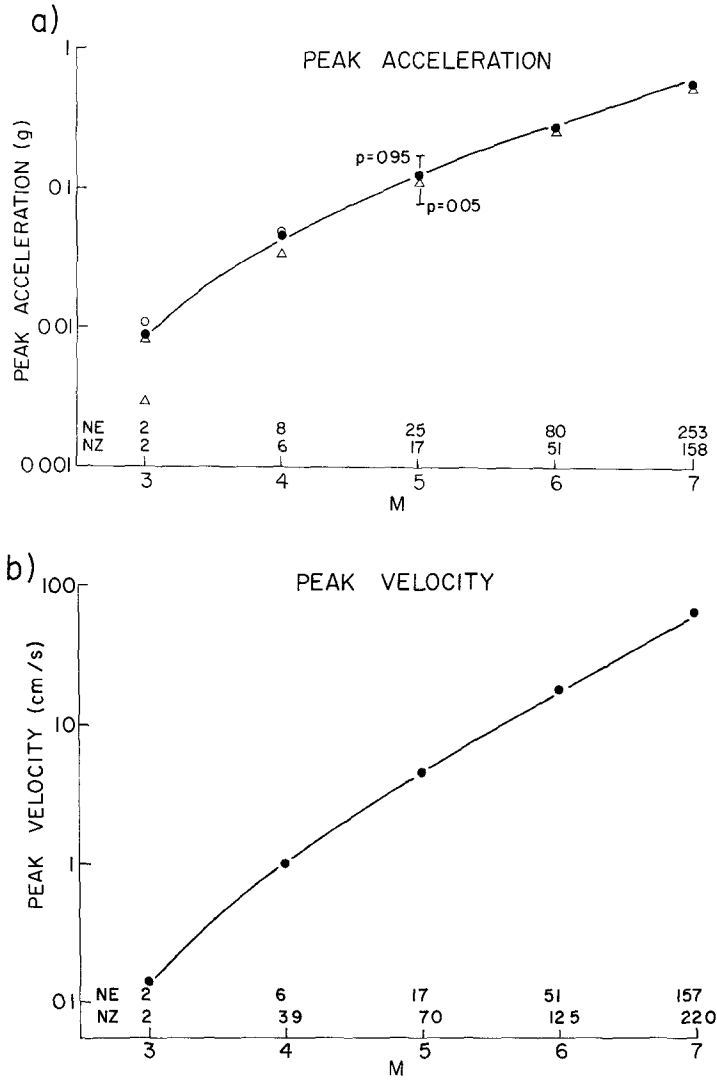


FIG. 14. Predictions of peak acceleration and peak velocity magnitude scaling from time-domain simulations (solid line) and random vibration theory [open circles: equation (24); closed circles: equation (21) for small N , equation (24) for large N ; squares: equation (B1) with $p = 1/e$; triangles: equation (B2) with $p = 1/e$]. The vertical bars for $M = 5$ outline the interval spanned by equations (B1) and (B2), with $p = 0.05$ and 0.95 (this approximates the 90 per cent confidence interval). Peak velocities have been computed from equations (21) and (24) only. Also shown are the values used in the random vibration theory for the number of extrema (NE) and the number of positive zero crossings (NZ).

use the random vibration theory, for it depends only on various moments of the spectrum (and on a choice of T). It is interesting to note that the equation used by Hanks and McGuire (1981)—equation (18)—works as well as equation (24) for peak acceleration, but for reasons of serendipity: the underestimation resulting from

using only the first term of the asymptotic expansion is compensated by an overestimation of the predominant frequency, and thus N . For the model parameters used in this paper, the predominant frequency estimated by equation (27) ranges from 13 to 8 Hz for a range of magnitudes from 3 to 7, when $f_m = 15$ Hz (the predominant frequency that would have been used by Hanks and McGuire). Although the errors in using only the first term of equation (24) and in estimating the predominant frequency by f_m [i.e., equation (20)] can be several tens of a per cent,

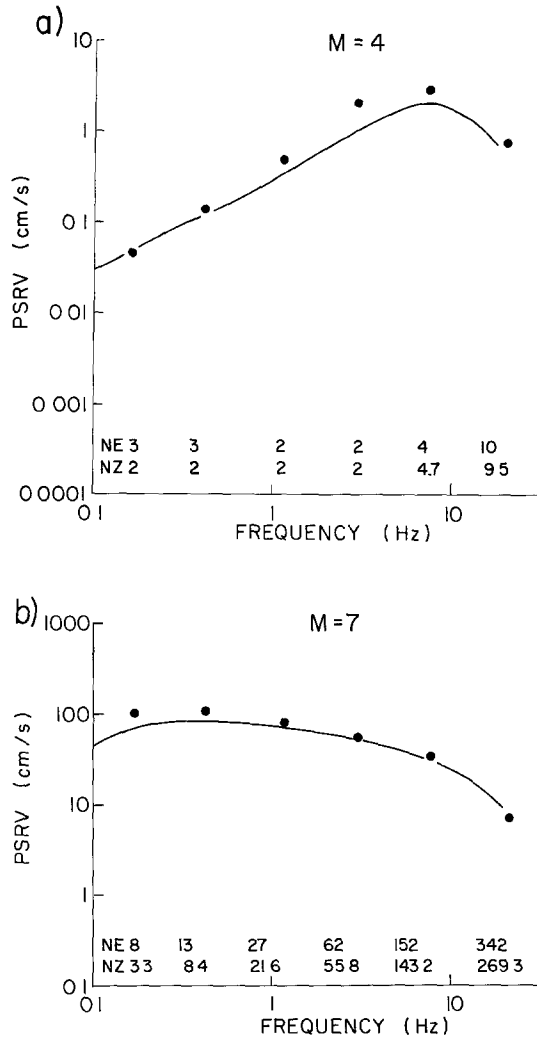


FIG. 15. Predictions of 5 per cent damped response spectra from time-domain simulations (solid line) and random vibration theory (dots).

the final estimates of peak acceleration differ by only several percent. Because the quantity m_2 need not be computed, the estimates of peak acceleration based on equations (18) and (20) are particularly convenient to use.

DISCUSSION AND CONCLUSIONS

A simple method has been proposed to simulate strong ground motions. The essence of the method is to generate a filtered, stochastic finite-duration time series

whose amplitude spectrum is equal, on the average, to a theoretical spectrum. To be useful, the theoretical spectrum and its scaling with earthquake size should have a sound physical basis. Although any spectral shape and scaling could be used, I have followed Hanks and McGuire (1981) in using an ω -squared spectrum with a high-frequency cutoff and a constant stress parameter. I have shown that this spectral model accounts for essentially all important measures of strong ground motion, measures based on the analysis of hundreds of recordings from earthquakes in western North America. The model is also in reasonable agreement with peak velocities and accelerations from small earthquakes recorded by McGarr *et al.* (1981) in a South African gold mine (see note 2 added in proof).

The model as given here may break down for predictions of motions close to large earthquakes, where the point source approximation is not valid and where the assumed spectral scaling with one low-frequency corner frequency is probably no longer appropriate. Recently, Joyner (1983) has devised a source scaling model that is intended to apply to large (as well as small) earthquakes. His model assumes geometrical similarity up to a certain critical earthquake size at which the rupture breaks the entire width of the seismogenic zone. Beyond that size, the fault length increases, but the width remains constant. For earthquakes smaller than the critical earthquake, Joyner's predictions of peak motions are similar to those from the model in this paper, the predicted motions from the two models diverge at larger magnitudes, with his predicted ground motion values increasing more slowly with magnitude.

Although the point source approximation is justified for the comparisons with data made in this paper, its validity is difficult to assess for predictions of motions close to large earthquakes. In a sense, the decaying exponential in the window function can be thought of as accounting for the extra decay of motions radiated from farther regions of the fault, but modifications may be required for predictions close to extended faults. These modifications may amount simply to redefining the window based on a kinematic model of the rupture (e.g., Midorikawa and Kobayashi, 1978), or to subdividing the fault into a series of equivalent point sources.

Among other uses, the simulation method offers a way of predicting motions for a particular design earthquake from recordings of smaller events in the region of interest—the small events being used to estimate the parameters f_m and $\Delta\sigma$. Such a use would be particularly valuable in the Central and Eastern United States, where recordings are usually available only for earthquakes with magnitudes smaller than the design earthquakes of important engineered structures.

Although the simulation method is useful for applications requiring one or more time series, it is a cumbersome way of predicting various peak measures of ground motion. For this, I show that with the possible exception of small earthquakes, various formulas from random vibration theory are adequate for predicting peak values. These formulas are particularly convenient, for they only require various integrals of the squared amplitude spectra and an estimate of the record duration. Estimates of the ground motions can be derived from them at much less cost than they can from the time series simulations.

ACKNOWLEDGMENTS

I thank T. C. Hanks for the motivation to do this work and T. C. Hanks, W. B. Joyner, and J. Boatwright for stimulating discussion along the way. D. J. Andrews, K. W. Campbell, T. C. Hanks, W. B. Joyner, M. W. McCann, Jr., A. McGarr, and C. S. Mueller provided thoughtful reviews of the manuscript. The response spectra were computed with a program written by A. Chen.

REFERENCES

- Aki, K (1967). Scaling law of seismic spectrum, *J Geophys. Res* **72**, 1217-1231
- Boatwright, J. (1982). A dynamic model for far-field acceleration, *Bull Seism Soc. Am* **72**, 1049-1068.
- Boore, D. M. (1980). On the attenuation of peak velocity, *Proc. of 7th World Conf on Earthquake Eng.*, 577-584.
- Boore, D. M (1983) Strong-motion seismology, *Rev Geophys Space Phys* **21**, 1308-1318
- Boore, D. M. and W. B. Joyner (1983). Ground motions and response spectra at soil sites from seismological models of radiated spectra, *U.S. Geol. Surv Open-File Rept* (in press).
- Bouchon, M. (1978). A dynamic source model for the San Fernando earthquake, *Bull. Seism. Soc. Am* **68**, 1555-1576.
- Brune, J. N. (1970). Tectonic stress and the spectra of seismic shear waves from earthquakes, *J. Geophys Res* **75**, 4997-5009.
- Brune, J. N. (1971). Correction, *J Geophys. Res* **76**, 5002.
- Campbell, K. W. (1981). Near source attenuation of peak horizontal acceleration, *Bull Seism Soc Am* **71**, 2039-2070.
- Cartwright, D. E. and M. S. Longuet-Higgins (1956) The statistical distribution of the maxima of a random function, *Proc. Roy Soc. London, Ser A237*, 212-223
- Clough, R. W. and J. Penzien (1975). *Dynamics of Structures*, McGraw-Hill, New York, 634 pp
- Davenport, A. G. (1964). Note on the distribution of the largest value of a random function with application to gust loading, *Proc Institution of Civil Engineers* **28**, 187-196.
- Hanks, T. C (1979a). Seismological aspects of strong motion seismology, *Proc. of the 2nd U.S. Natl Conf on Earthquake Eng.*, convened Stanford Univ., Aug. 22-24, 1979, 898-912.
- Hanks, T. C. (1979b). b values and $\omega^{-\gamma}$ seismic source models: implications for tectonic stress variations along active crustal fault zones and the estimation of high frequency strong ground motion, *J Geophys Res* **84**, 2235-2241.
- Hanks, T. C. (1982). f_{max} , *Bull Seism Soc. Am* **72**, 1867-1879
- Hanks, T. C. and H. Kanamori (1979). A moment magnitude scale, *J. Geophys. Res* **84**, 2348-2350.
- Hanks, T. C. and R. K. McGuire (1981). The character of high frequency strong ground motion, *Bull Seism Soc. Am* **71**, 2071-2095.
- Herrmann, R. B. and M. J. Goertz (1981). A numerical study of peak ground motion scaling, *Bull Seism Soc Am* **71**, 1963-1979.
- Iyengar, R. N. and K. T. S. R. Iyengar (1969). A nonstationary random process model for earthquake accelerograms, *Bull Seism Soc Am* **59**, 1163-1188.
- Jennings, P. C. and H. Kanamori (1983) Effect of distance on local magnitude found from strong-motion records, *Bull Seism Soc. Am* **73**, 265-280.
- Joyner, W. B. (1983) A proposed scaling law for the spectra of large earthquakes (submitted for publication).
- Joyner, W. B. and D. M. Boore (1980). A stochastic source model for synthetic strong motion seismograms, *Proc of 7th World Conf on Earthquake Eng.*, 1-8.
- Joyner, W. B. and D. M. Boore (1981). Peak horizontal acceleration and velocity from strong motion records including records from the 1979 Imperial Valley, California, earthquake, *Bull Seism Soc Am* **71**, 2011-2038.
- Joyner, W. B. and D. M. Boore (1982) Prediction of earthquake response spectra, *U.S. Geol. Surv., Open-File Rept* 82-977, 16 pp
- Kanamori, H. and P. C. Jennings (1978). Determination of local magnitude, M_L , from strong motion accelerograms, *Bull Seism Soc Am* **68**, 471-485
- Luco, J. E. (1982) A note on near-source estimates of local magnitude, *Bull. Seism Soc Am* **72**, 941-958.
- McGarr, A. R., W. E. Green, and S. M. Spottiswoode (1981). Strong ground motion of mine tremors: some implications for near source ground motion parameters, *Bull. Seism. Soc. Am* **71**, 295-319.
- McGuire, R. K. and T. C. Hanks (1980). RMS accelerations and spectral amplitudes of strong ground motion during the San Fernando, California earthquake, *Bull Seism. Soc Am* **70**, 1907-1919
- Midorikawa, S. and H. Kobayashi (1978). On the estimation of strong earthquake motions with regard to fault rupture, *Proc. of the Second Int Conf on Microzonation* (convened San Francisco, Calif., Nov 26-Dec 1, 1978) **2**, 825-836.
- Nau, R. F., R. M. Olver, and K. S. Pister (1982). Simulating and analyzing artificial nonstationary earthquake ground motions, *Bull Seism Soc. Am* **72**, 615-636.
- Papageorgiou, A. S. and K. Aki (1983) A specific barrier for the quantitative description of inhomogeneous faulting and the prediction of strong ground motion II Applications of the model, *Bull. Seism Soc Am* **73**, 953-978.

- Saragoni, G. R. and G. C. Hart (1974). Simulation of artificial earthquakes, *Earthquake Eng. Structural Dyn* **2**, 249–267.
- Seekins, L. C. and T. C. Hanks (1978). Strong-motion accelerograms of the Oroville aftershocks and peak acceleration data, *Bull Seism. Soc. Am* **68**, 677–689.
- Udwadia, F. E. and M. D. Trifunac (1974). Characterization of response spectra through the statistics of oscillator response, *Bull Seism Soc Am*. **64**, 205–219.
- Vanmarcke, E. H. (1976) Structural response to earthquakes, in *Seismic Risk and Engineering Decisions*, ch 8, C Lomnitz and E Rosenblueth, Editors, Elsevier Publishing Co., Amsterdam, 287–337.
- Vanmarcke, E. H. and S P Lai (1980) Strong-motion duration of earthquakes, *Bull Seism Soc Am* **70**, 1293–1307

U.S. GEOLOGICAL SURVEY
 OFFICE OF EARTHQUAKES, VOLCANOES AND ENGINEERING
 345 MIDDLEFIELD ROAD
 MENLO PARK, CALIFORNIA 94025

Manuscript received 22 March 1983

APPENDIX A: SCALING RELATIONS FOR PEAK ACCELERATION AND PEAK VELOCITY

A simplified analytic form of the scaling of peak acceleration and velocity with moment magnitude can be derived easily from the equations in the section on random vibration theory. The equation for peak acceleration has been published by Hanks and McGuire (1981), and its derivation is repeated here for completeness. The goal here is to find the moment magnitude coefficients γ in the equations

$$\log(a_{\max}) = \gamma_a M + \eta_a \tag{A1a}$$

and

$$\log(v_{\max}) = \gamma_v M + \eta_v. \tag{A1b}$$

Only those portions of the intercept values η that depend on the stress parameter $\Delta\sigma$ will be estimated; distance-dependent terms will be ignored. This reduces the clutter in the ensuing equations and simplifies some of the integrations [for example, the Q -term in equation (1) can be ignored]. In predicting the absolute level of the peak motions, it is best (and easy) to numerically evaluate the integrals used in the random vibration theory.

The simple asymptotic relation between the peak and rms motion given by equation (18) will be used, and equation (25) will be used to compute the rms. The basic task is to compute the integral measures m_0 , m_2 for the acceleration and velocity spectra. This amounts to doing the integrals

$$(m_k)_l \sim M_0^2 \int_0^{\omega_m} \omega^k \left[\frac{\omega^l}{1 + (\omega/\omega_c)^2} \right]^2 d\omega \tag{A2}$$

where $k = 0, 2$ and $l = 1$ for velocity and $l = 2$ for acceleration. Defining $x \equiv \omega/\omega_c$, the integral above can be rewritten

$$(m_k)_l \sim M_0^2 \omega_c^{k+2l+1} \int_0^{\omega_m/\omega_c} \frac{x^{k+2l}}{[1 + x^2]^2} dx. \tag{A3}$$

Although this integral can be evaluated analytically, a simplification is possible when $\omega_m/\omega_c \gg 1$: the 1 in the denominator can generally be ignored and then

$$(m_k)_l \sim M_0^2 \omega_c^{k+2l+1} \int_0^{\omega_m/\omega_c} x^{k+2l-4} dx \tag{A4}$$

and, finally,

$$(m_k)_l \sim M_0^2 \omega_c^{k+2l+1} (\omega_m/\omega_c)^{k+2l-3}. \tag{A5a}$$

This equation is not valid for the zeroth moment ($k = 0$) of the velocity spectrum ($l = 1$), for then the superscript of x in equation (A4) is negative. In this case equation (A5b) must be replaced by

$$(m_0)_1 \sim \frac{\pi}{4} M_0^2 \omega_c^3. \tag{A5b}$$

Using equations (25) and (6) and changing from radian frequency to the more familiar circular frequency, the dependence of the rms motions on M_0 and f_c then becomes

$$a_{rms} \sim M_0 f_c^3 \left(\frac{f_m}{f_c}\right)^{1/2} \tag{A6a}$$

and

$$v_{rms} \sim M_0 f_c^2. \tag{A6b}$$

The estimate of the predominant frequency \tilde{f} comes from equation (27). For acceleration,

$$\tilde{f} = f_m \tag{A7a}$$

and for velocity,

$$\tilde{f} = \frac{2}{\sqrt{\pi}} \left(\frac{f_m}{f_c}\right)^{1/2} f_c. \tag{A7b}$$

Using equations (18) for a_{max}/a_{rms} , equation (19) for N , and equation (6) for T , the estimates for a_{max} and v_{max} become

$$a_{max} \sim M_0 f_c^3 (f_m/f_c)^{1/2} \sqrt{\ln(2f_m/f_c)} \tag{A8a}$$

and

$$v_{max} \sim M_0 f_c^2 \sqrt{\ln\left(\frac{16}{\pi} \frac{f_m}{f_c}\right)}. \tag{A8b}$$

The next step is to write f_c in terms of M_0 and $\Delta\sigma$ [equation (5)]. Because the logarithm of equation (A8) is of interest, constant factors associated with the terms outside the square root can be ignored. Therefore

$$\log(a_{\max}) \sim \frac{1}{6} \log M_0 + \frac{5}{6} \log \Delta\sigma + \frac{1}{2} \log \left[\ln \left(2 \frac{f_m}{\xi} \left(\frac{M_0}{\Delta\sigma} \right)^{1/3} \right) \right] \tag{A9a}$$

and

$$\log(v_{\max}) \sim \frac{1}{3} \log M_0 + \frac{2}{3} \log \Delta\sigma + \frac{1}{2} \log \left[\ln \left(\frac{16}{\pi} \frac{f_m}{\xi} \left(\frac{M_0}{\Delta\sigma} \right)^{1/3} \right) \right] \tag{A9b}$$

where $\xi = 4.9 \times 10^6 \beta$ [equation (5)]. The first and second terms give the scaling of the rms motions with M_0 and $\Delta\sigma$; the last terms give modifications to the scaling

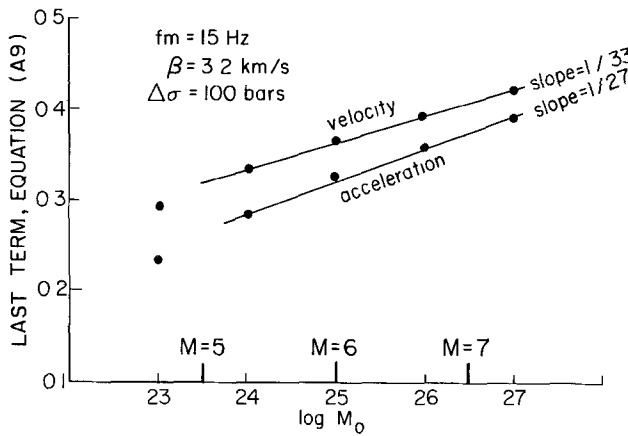


FIG. A1. Dependence of second term in equations (A9) on $\log M_0$.

due to the distribution of motions over a time interval. Following Hanks and McGuire (1981), the last terms on the right-hand sides of equations (A9) can be approximated by terms linear in $\log \Delta\sigma$ and $\log M_0$. For example, the last terms have been plotted in Figure A1 as a function of $\log M_0$ for $f_m = 15$ Hz, $\beta = 3.2$ km/sec, and $\Delta\sigma = 100$ bars. The term corresponding to peak acceleration has more curvature than that for peak velocity, but in both cases the terms can be approximated by straight lines, as shown. Substituting these straight line approximations, and similar ones for the $\Delta\sigma$ dependence, into equations (A9) and using the definition of moment magnitude [equation (12)], the scaling of peak acceleration and peak velocity with moment magnitude and the stress parameter is given approximately by

$$\log(a_{\max}) \sim 0.31M + 0.80 \log \Delta\sigma \tag{A10a}$$

and

$$\log(v_{\max}) \sim 0.55M + 0.64 \log \Delta\sigma. \tag{A10b}$$

The effect of the random process is to slightly increase and decrease the dependence of peak acceleration and velocity on M and $\Delta\sigma$, respectively, relative to the scaling of the rms motions. The largest effect is on the magnitude dependence of peak acceleration. Rounded to one decimal place, the first terms in equations (A10) give the magnitude dependence shown in equations (17) in the text.

APPENDIX B: RANDOM VIBRATION THEORY EQUATIONS

Udwadia and Trifunac (1974) gave the following equation for the maximum amplitude that has a probability p of not being exceeded

$$\frac{a_{\max,p}}{a_{\text{rms}}} = [-2 \ln(1 - p^{1/N})]^{1/2}. \quad (\text{B1})$$

The corresponding equation from Vanmarcke (1976) is

$$\frac{a_{\max,p}}{a_{\text{rms}}} = [2 \ln(n)[1 - \exp(-\delta_e \sqrt{\pi \ln(n)})]^{1/2} \quad (\text{B2})$$

where

$$n = N(-\ln p)^{-1} \quad (\text{B3})$$

$$\delta_e = \delta_y^{1/2} \quad (\text{B4})$$

and

$$\delta_y = (1 - m_1^2/m_0m_2)^{1/2}. \quad (\text{B5})$$

For large N , equations (B1) and (B2) approach

$$\frac{a_{\max,p}}{a_{\text{rms}}} = [2 \ln(n)]^{1/2}. \quad (\text{B6})$$

When $p = 1/e$, this is the same as equation (18) in the text.

Notes Added in Proof

1. Recent work by myself and W. Joyner on an algorithm for choosing the oscillator durations leads to an improved fit between the time domain simulations and the random vibration theory shown in Figure 15. This work will be reported on in a later paper.
2. In a paper recently submitted to the *Journal of Geophysical Research*, T. Hanks and I show that the model is consistent with the correlation between $\log M_0$ and M_L from an extensive California earthquake dataset for $0 < M_L < 7$.